

1 LEVERAGING MULTI-MESSENGER ASTROPHYSICS FOR DARK MATTER SEARCHES

By

Daniel Nicholas Salazar-Gallegos

A DISSERTATION

Submitted to
Michigan State University
in partial fulfillment of the requirements
for the degree of

Physics—Doctor of Philosophy
Computational Mathematics in Science and Engineering—Dual Major

Today

ABSTRACT

3 I did Dark Matter with HAWC and IceCube. I also used Graph Neural Networks

⁴ Copyright by

⁵ DANIEL NICHOLAS SALAZAR-GALLEGOS

⁶ Today

ACKNOWLEDGMENTS

8 I love my friends. Thanks to everyone that helped me figure this out. Amazing thanks to the people
9 at LANL who supported me. Eames, etc Dinner Parties Jenny and her child Kaydince Kirsten, Pat,
10 Andrea Family. You're so far but so critical to my formation. Unconditional love. Roommate

TABLE OF CONTENTS

12	LIST OF TABLES	vi
13	LIST OF FIGURES	vii
14	LIST OF ABBREVIATIONS	ix
15	CHAPTER 1 INTRODUCTION	1
16	CHAPTER 2 DARK MATTER IN THE COSMOS	2
17	2.1 Introduction	2
18	2.2 Dark Matter Basics	3
19	2.3 Evidence for Dark Matter	4
20	2.4 Searching for Dark Matter: Particle DM	11
21	2.5 Sources for Indirect Dark Matter Searches	16
22	2.6 Multi-Messenger Dark Matter	18
23	CHAPTER 3 MULTIMESSENGER ASTROPHYSICS: DETECTING HIGH EN-	
24	ERGY NEUTRAL MESSENGERS	21
25	3.1 Introduction	21
26	3.2 Charged Particles in a Medium	21
27	3.3 Photons (γ)	22
28	3.4 Neutrinos (ν)	22
29	3.5 Opportunities to Combine for Dark Matter	22
30	CHAPTER 4 HIGH ALTITUDE WATER CHERENKOV (HAWC) OBSERVATORY .	24
31	4.1 The Detector	24
32	4.2 Events Reconstruction and Data Acquisition	24
33	4.3 Remote Monitoring	24
34	CHAPTER 5 ICECUBE NEUTRINO OBSERVATORY	25
35	5.1 The Detector	25
36	5.2 Events Reconstruction and Data Acquisition	25
37	5.3 Northern Test Site	25
38	CHAPTER 6 COMPUTATIONAL TECHNIQUES IN PARTICLE ASTROPHYSICS .	26
39	6.1 Neural Networks for Gamma/Hadron Separation	26
40	6.2 Parallel Computing for Dark Matter Analyses	26
41	CHAPTER 7 GLORY DUCK	27
42	7.1 Dataset and Background	27
43	7.2 Analysis	29
44	CHAPTER 8 NU DUCK	33
45	BIBLIOGRAPHY	34

LIST OF TABLES

47 Table 7.1 Summary of the relevant properties of the dSphs used in the present work. 48 Column 1 lists the dSphs. Columns 2 and 3 present their heliocentric distance 49 and galactic coordinates, respectively. Columns 4 and 5 report the J -factors of 50 each source given from the \mathcal{GS} and \mathcal{B} independent studies and their estimated 51 $\pm 1\sigma$ uncertainties. The values $\log_{10} J$ (\mathcal{GS} set) [30] correspond to the mean 52 J -factor values for a source extension truncated at the outermost observed star. 53 The values $\log_{10} J$ (\mathcal{B} set) [31] are provided for a source extension at the tidal 54 radius of each dSph. Bolded sources are within HAWC's field of view and 55 provided to the Glory Duck analysis. 31
56 Table 7.2 Summary of dSph observations by each experiment used in this work. A 57 ‘-’ indicates the experiment did not observe the dSph for this study. For 58 Fermi-LAT, the exposure at 1 GeV is given. For HAWC, $ \Delta\theta $ is the absolute 59 difference between the source declination and HAWC latitude. HAWC is more 60 sensitive to sources with smaller $ \Delta\theta $. For IACTs, we show the zenith angle 61 range, the total exposure, the energy range, the angular radius θ of the signal or 62 ON region, the ratio of exposures between the background-control (OFF) and 63 signal (ON) regions (τ), and the significance of gamma-ray excess in standard 64 deviations, σ 32
65 Proof I know how to include	

LIST OF FIGURES

<p>67 Figure 2.1 Rotation curve fit to NGC 6503 from [7]. Dashed line is the contribution 68 from visible matter. Dotted curves are from gas. Dash-dot curves are from 69 dark matter (DM). Solid line is the composite contribution from all matter 70 and DM sources. Data are indicated with bold dots with error bars. Data 71 agree strongly with a matter + DM composite prediction.</p> <p>72 Figure 2.2 Light from distant galaxy is bent in unique ways depending on the distribution 73 of mass between the galaxy and Earth. Yellow dashed lines indicate where 74 the light would have gone if the matter were not present [8].</p> <p>75 Figure 2.3 (left) Optical image of galactic cluster 1E0657-558. (right) X-ray image of the 76 cluster with redder meaning hotter and higher baryon density. (both) Green 77 contours are reconstruction of gravity contours from weak lensing. White 78 rings are the best fit mass maxima at 68.3%, 95.5%, and 99.7% confidence. 79 The matter maxima of the clusters are clearly separated from x-ray maxima. [9]</p> <p>80 Figure 2.4 Plank CMB sky. Sky map features small variations in temperature in primor- 81 dial light. These anisotropies are used to make inferences about the universe's 82 energy budget and developmental history. [10]</p> <p>83 Figure 2.5 Observed Cosmic Microwave Background power spectrum as a function of 84 multipole moment from Plank [10]. Blue line is best fit model from ΛCDM. 85 Red points and lines are data and error, respectively.</p> <p>86 Figure 2.6 Predicted power spectra of CMB for different $\Omega_m h^2$ values for fixed baryon 87 density from [11]. (left) Low $\Omega_m h^2$ increases the prominence of first and 88 second peaks. (middle) $\Omega_m h^2$ is most similar to the observed power spectrum. 89 The second and third peaks are similar in height. (right) $\Omega_m h^2$ is large which 90 suppresses the first peak and raises the prominence of the third peak.</p> <p>91 Figure 2.7 The Standard Model (SM) of particle physics. Figure taken from http://www.quantumdiaries.org/2014/03/14/the-standard-model-a-beautiful-but-flawed-theory/</p> <p>94 Figure 2.8 Simplified Feynman diagram demonstrating with different ways DM can 95 interact with SM particles. The 'X's refer to the DM particles whereas the 96 SM refer to fundamental particles in the SM. The large circle in the center 97 indicates the vertex of interaction and is purposely left vague. The colored 98 arrows refer to different directions of time as well as their respective labels. 99 The arrows indicate the initial and final state of the DM -SM interaction in time.</p>	<p>5</p> <p>7</p> <p>8</p> <p>9</p> <p>10</p> <p>10</p> <p>12</p> <p>13</p>
--	---

100	Figure 2.9 A single jet event in ATLAS detector from 2017 [16]. Jet momentum was 101 observed to be 1.9 TeV. Missing transverse momentum was observed to be 102 1.9 TeV compared to the initial transverse momentum of the event was 0. 103 Implied MET is traced by a red dashed line in event display.	14
104	Figure 2.10 More detailed pseudo-Feynman diagram of particle cascade from dark matter 105 annihilation into 2 quarks. The quarks hadronize and down to stable particles 106 like γ or the anti-proton (p^-). Diagram pulled from ICRC 2021 presentation 107 on DM annihilation search [17].	15
108	Figure 2.11 Dark Matter (DM) decay spectrum for $b\bar{b}$ initial state and γ final state. Redder 109 spectra are for larger DM masses. Bluer spectra are light DM masses. x is a 110 unitless factor defined as the ratio of the mass of DM, m_χ , and the final state 111 particle energy E_γ . Figure from [19].	17
112	Figure 2.12 Different dark matter density profiles compared. Some models produce ex- 113 ceptionally large densities at small r [20].	18
114	Figure 2.13 The Milky Way Galaxy in photons (γ) and neutrinos (ν) [22]. The Galactic 115 center is at $l=0^\circ$ and is the brightest region in all panels. (top) An Optical 116 color image of the Milky Way galaxy seen from Earth. Clouds of gas and dust 117 obscure some light from stars. (2nd down) Integrated flux of γ -rays observed 118 by the Fermi-LAT telescope [23]. (middle) Expected neutrino emission 119 that corresponds with Fermi-LAT observations. (2nd up) Expected neutrino 120 emission profile after considering detector systematics of IceCube. (bottom) 121 Observed neutrino emission from region of the galactic plane. Substantial 122 neutrino emission was detected.	19
123	Figure 2.14 Dark Matter annihilation spectra for different final state particle and standard 124 model annihilation channels [24]. Photons (red), e^\pm (green), \bar{p} (blue), ν (black).	20
125	Figure 3.1 TODO: Show a nuclear reactor with cherenkov radiation[NEEDS A SOURCE][FACT 126 CHECK THIS]	22
127	Figure 3.2 TODO: absorption spectrum of liquid and solid water[NEEDS A SOURCE][FACT 128 CHECK THIS]	23

LIST OF ABBREVIATIONS

- 130 **MSU** Michigan State University
131 **LANL** Los Alamos National Laboratory
132 **DM** Dark Matter
133 **SM** Standard Model
134 **HAWC** High Altitude Water Cherenkov Observatory

135

CHAPTER 1

INTRODUCTION

136 Is the text not rendering right? Ah ok it knows im basically drafting the doc still

CHAPTER 2

137

DARK MATTER IN THE COSMOS

138 **2.1 Introduction**

139 The dark matter problem can be summarized in part by the following thought experiment.

140 Let us say you are the teacher for an elementary school classroom. You take them on a field
141 trip to your local science museum and among the exhibits is one for mass and weight. The exhibit
142 has a gigantic scale, and you come up with a fun problem for your class.

143 You ask your class, "What is the total weight of the classroom? Give your best estimation to
144 me in 30 minutes, and then we'll check your guess on the scale. If your guess is within 10% of the
145 right answer, we will stop for ice cream on the way back."

146 The students are ecstatic to hear this, and they get to work. The solution is some variation of
147 the following strategy. The students should give each other their weight or best guess if they do
148 not know. Then, all they must do is add each student's weight and get a grand total for the class.
149 The measurement on the giant scale should show the true weight of the class. When comparing
150 the measured weight to your estimation, multiply the measurement by 1.0 ± 0.1 to get the $\pm 10\%$
151 tolerances for your estimation.

152 Two of your students, Sandra and Mario, return to you with a solution.

153 They say, "We weren't sure of everyone's weight. We used 65 lbs. for the people we didn't
154 know and added everyone who does know. There are 30 of us, and we got 2,000 lbs.! That's a ton!"

155 You estimated 1,900 lbs. assuming the average weight of a student in your class was 60 lbs.
156 So, you are pleased with Sandra's and Mario's answer. You instruct your students to all gather on
157 the giant scale and read off the weight together. To all your surprise, the scale reads *10,000 lbs.!*
158 10,000 is significantly more than a 10% error from 2,000. In fact, it is approximately 5 times more
159 massive than either your or your students' estimates. You think to yourself and conclude there
160 must be something wrong with the scale. You ask an employee to check the scale and verify it is
161 well calibrated. They confirm that the scale is in working order. You weigh a couple of students
162 individually to assess that the scale is well calibrated. Sandra weighs 59 lbs., and Mario weighs

163 62 lbs., typical weights for their age. You then weigh each student individually and see that their
164 weights individually do not deviate greatly from 60 lbs. So, where does all the extra weight come
165 from?

166 This thought experiment serves as an analogy to the Dark Matter problem. The important
167 substitution to make however is to replace the students with stars and the classroom with a galaxy,
168 say the Milky Way. Individually the mass of stars is well measured and defined with the Sun as our
169 nearest test case. However, when we set out to measure the mass of a collection of stars as large as
170 galaxies, our well-motivated estimation is wildly incorrect. There simply is no way to account for
171 this discrepancy except without some unseen, or dark, contribution to mass and matter in galaxies.
172 I set out in my thesis to narrow the possibilities of what this Dark Matter could be.

173 This chapter is organized like the following... **TODO: Text should look like ... Chapter x has**
174 **blah blah blah.**

175 2.2 Dark Matter Basics

176 Presently, a more compelling theory of cosmology that includes Dark Matter (DM) in order
177 to explain a variety of observations is Λ Cold Dark Matter, or Λ CDM. I present the evidence
178 supporting Λ CDM in Section 2.3 yet discuss the conclusions of the Λ CDM model here. According
179 to Λ CDM fit to observations on the Cosmic Microwave Background (CMB), DM is 26.8% of the
180 universe's current energy budget. Baryonic matter, stuff like atoms, gas, and stars, contributes to
181 4.9% of the universe's current energy budget [1, 2, 3].

182 DM is dark; it does not interact readily with light at any wavelength. DM also does not interact
183 noticeably with the other standard model forces (Strong and Weak) at a rate that is readily observed
184 [3]. DM is cold, which is to say that the average velocity of DM is below relativistic speeds [1].
185 'Hot' DM would not likely manifest the dense structures we observe like galaxies, and instead
186 would produce much more diffuse galaxies than what is observed [3, 1]. DM is old; it played a
187 critical role in the formation of the universe and the structures within it [1, 2].

188 Observations of DM have so far been only gravitational. The parameter space available to what
189 DM could be therefore is extremely broad. The broad DM parameter space is iteratively tested in

190 DM searches by supposing a hypothesis that has not yet been ruled out and performing observations
191 to test them. When the observations yield a null result, the parameter space is constrained further.
192 I present some approaches for DM searches in Section 2.4.

193 **2.3 Evidence for Dark Matter**

194 Dark Matter (DM) has been a looming problem in physics for almost 100 years. Anomalies
195 have been observed by astrophysicists in galactic dynamics as early as 1933 when Fritz Zwicky
196 noticed unusually large velocity dispersion in the Coma cluster. Zwicky's measurement was the
197 first recorded to use the Virial theorem to measure the mass fraction of visible and invisible matter
198 in celestial bodies [4]. From Zwicky in [5], "*If this would be confirmed, we would get the surprising*
199 *result that dark matter is present in much greater amount than luminous matter.*" Zwicky's and
200 others' observation did not instigate a crisis in astrophysics because the measurements did not
201 entirely conflict with their understanding of galaxies [4]. In 1978, Rubin, Ford, and Norbert
202 measured rotation curves for ten spiral galaxies [6]. Rubin et al.'s 1978 publication presented a
203 major challenge to the conventional understanding of galaxies that could no longer be dismissed by
204 measurement uncertainties. Evidence has been mounting ever since for this exotic form of matter.
205 The following subsections provide three compelling pieces of evidence in support of the existence
206 of DM.

207 **2.3.1 First Clues: Stellar Velocities**

208 Zwicky, and later Rubin, measured the stellar velocities of various galaxies to estimate their
209 virial mass. The Virial Theorem upon which these observations are interpreted is written as

$$2T + V = 0. \quad (2.1)$$

210 Where T is the kinetic energy and V is the potential energy in a self-gravitating system. The
211 classical Newton's law of gravity from stars and gas was used for gravitational potential modeled in
212 the observed galaxies:

$$V = -\frac{1}{2} \sum_i \sum_{j \neq i} \frac{m_i m_j}{r_{ij}}. \quad (2.2)$$

213 Zwicky et al. measured just the velocities of stars apparent in optical wavelengths [5]. Rubin et al.
 214 added by measuring the velocity of the hydrogen gas via the 21 cm emission line of Hydrogen [6].
 215 The velocities of the stars and gas are used to infer the total mass of galaxies and galaxy clusters
 216 via Equation (2.1). An inferred mass is obtained from the luminosity of the selected sources. The
 217 two inferences are compared to each other as a luminosity to mass ratio which typically yielded [1]

$$\frac{M}{L} \sim 400 \frac{M_{\odot}}{L_{\odot}} \quad (2.3)$$

218 M_{\odot} and L_{\odot} referring to stellar mass and stellar luminosity, respectively. These ratios clearly indicate
 219 a discrepancy in apparent light and mass from stars and gas and their velocities.

220 Rubin et al. [6] demonstrated that the discrepancy was unlikely to be an underestimation of
 221 the mass of the stars and gas. The inferred "dark" mass was up to 5 times more than the luminous
 222 mass. This dark mass also needed to extend well beyond the extent of the luminous matter.

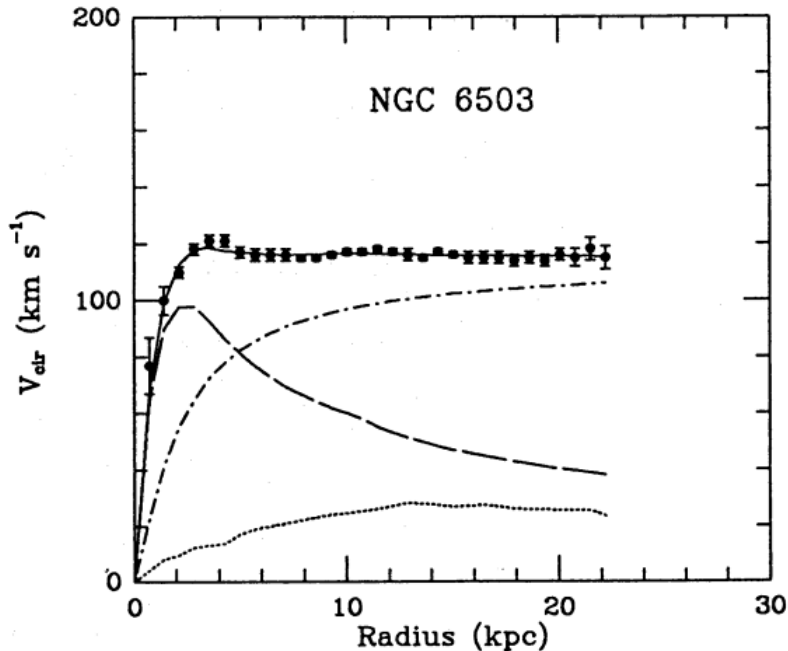


Figure 2.1 Rotation curve fit to NGC 6503 from [7]. Dashed line is the contribution from visible matter. Dotted curves are from gas. Dash-dot curves are from dark matter (DM). Solid line is the composite contribution from all matter and DM sources. Data are indicated with bold dots with error bars. Data agree strongly with a matter + DM composite prediction.

223 Figure 2.1 features one of many rotation curves plotted from the stellar velocities within galaxies.

224 The measured rotation curves mostly feature a flattening of velocities at higher radius which is not
225 expected if the gravity was only coming from gas and luminous matter. The extension of the
226 flat velocity region also indicates that the DM is distributed far from the center of the galaxy.
227 Modern velocity measurements include significantly larger objects, galactic clusters, and smaller
228 objects, dwarf galaxies. Yet, measurements along this regime are leveraging the Virial theorem
229 with Newtonian potential energies. We know Newtonian gravity is not a comprehensive description
230 of gravity. New observational techniques have been developed since 1978, and those are discussed
231 in the following sections.

232 **2.3.2 Evidence for Dark Matter: Gravitational Lensing**

233 Modern evidence for dark matter comes from new avenues beyond stellar velocities. Grav-
234 itational lensing from DM is a new channel from general relativity. General relativity predicts
235 aberrations in light caused by massive objects. In recent decades we have been able to measure the
236 lensing effects from compact objects and DM halos. Figure 2.2 shows how different massive ob-
237 jects change the final image of a faraway galaxy resulting from gravitational lensing. Gravitational
238 lensing developed our understanding of dark matter in two important ways.

239 Gravitational lensing provides additional compelling evidence for DM. The observation of two
240 merging galactic clusters in 2006, shown in Figure 2.3, provided a compelling argument for DM
241 outside the Standard Model. These clusters merged recently in astrophysical time scales. Galaxies
242 and star cluster have mostly passed by each other as the likelihood of their collision is low. Therefore,
243 these massive objects will mostly track the highest mass, dark and/or baryonic, density. Yet, the
244 intergalactic gas is responsible for the majority of the baryonic mass in the systems [4]. These gas
245 bodies will not phase through and will heat up as they collide together. The hot gas is located via
246 x-ray emission from the cluster. Two observations of the clusters were performed independently of
247 each other.

248 The first was the lensing of light around the galaxies due to their gravitational influences.
249 When celestial bodies are large enough, the gravity they exert bends space and time itself. The
250 warped space-time lenses light and will deflect in an analogous way to how glass lenses will bend

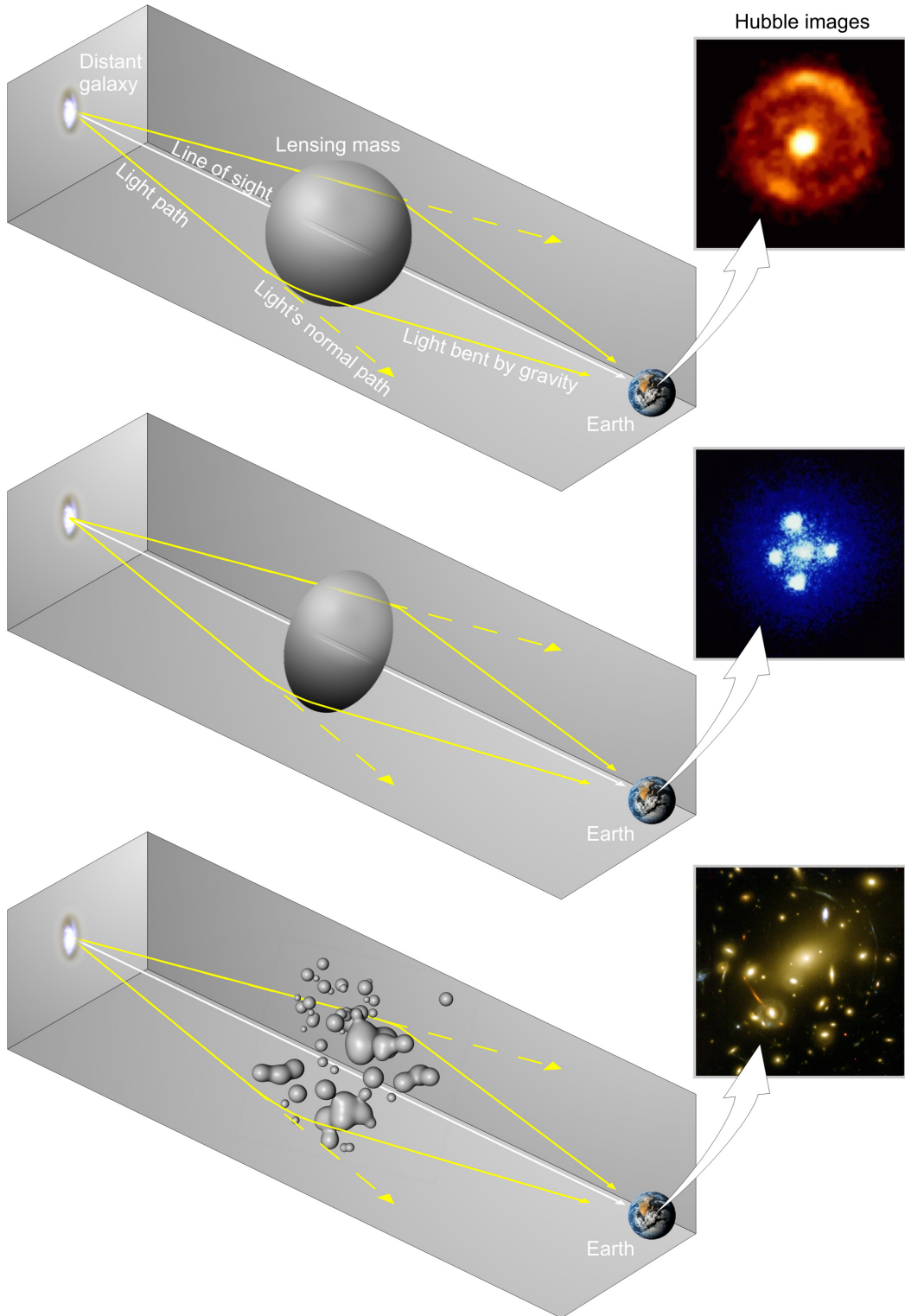


Figure 2.2 Light from distant galaxy is bent in unique ways depending on the distribution of mass between the galaxy and Earth. Yellow dashed lines indicate where the light would have gone if the matter were not present [8].

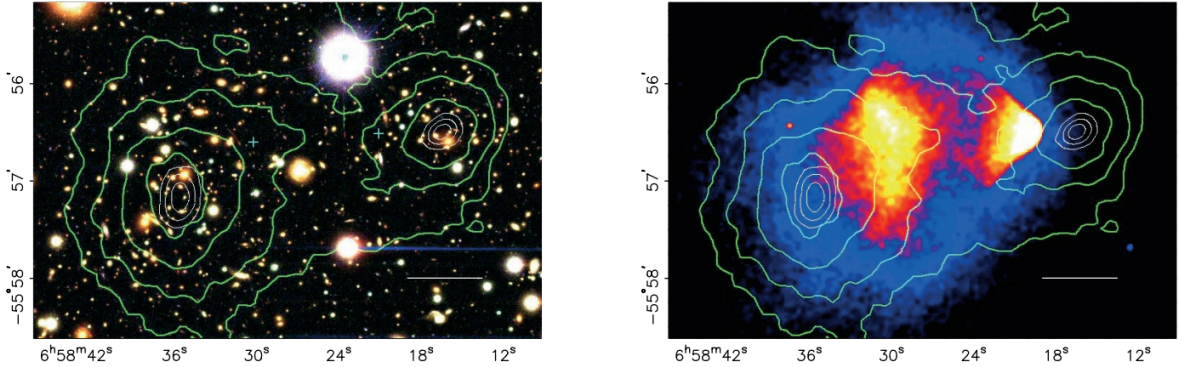


Figure 2.3 (left) Optical image of galactic cluster 1E0657-558. (right) X-ray image of the cluster with redder meaning hotter and higher baryon density. (both) Green contours are reconstruction of gravity contours from weak lensing. White rings are the best fit mass maxima at 68.3%, 95.5%, and 99.7% confidence. The matter maxima of the clusters are clearly separated from x-ray maxima. [9]

251 light, see Figure 2.2. With a sufficient understanding of light sources behind a massive object, we
 252 can reconstruct the contours of the gravitational lenses. The gradient of the contours shown in
 253 Figure 2.3 then indicates how dense the matter is and where it is.

254 The x-ray emission can then be observed from the clusters. Since these galaxies are mostly gas
 255 and are merging, then the gas should be getting hotter. If they are merging, the x-ray emissions
 256 should be the strongest where the gas is mostly moving through each other. Hence, X-ray emission
 257 maps out where the gas is in the merging galaxy cluster.

258 The lensing and x-ray observations were done on the Bullet cluster featured on Figure 2.3.
 259 The x-ray emissions do not align with the gravitational contours from lensing. The incongruence
 260 in mass density and baryon density suggests that there is a lot of matter somewhere that does
 261 not interact with light. Moreover, this dark matter cannot be baryonic [9]. The Bullet Cluster
 262 measurement did not really tell us what DM is exactly, but it did give the clue that DM also does
 263 not interact with itself very strongly. If DM did interact strongly with itself, then it would have been
 264 more aligned with the x-ray emission [9]. There have been follow-up studies of galaxy clusters with
 265 similar results. The Bullet Cluster and others like it provide a persuasive case against something
 266 possibly amiss in our gravitational theories.

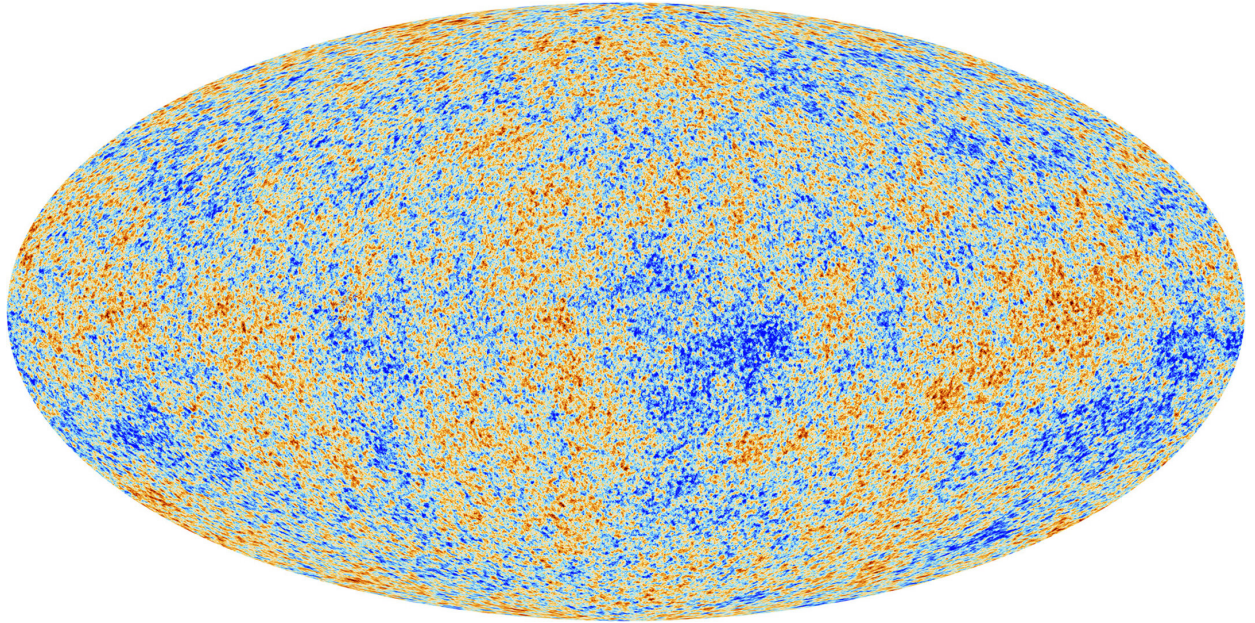


Figure 2.4 Plank CMB sky. Sky map features small variations in temperature in primordial light. These anisotropies are used to make inferences about the universe’s energy budget and developmental history. [10]

267 **2.3.3 Evidence for Dark Matter: Cosmic Microwave Background**

268 The Cosmic Microwave Background (CMB) is the primordial light from the early universe
269 when Hydrogen atoms formed from the free electron and proton soup in the early universe. The
270 CMB is the earliest light we can observe; released when the universe was about 380,000 years old.
271 Then we look at how the simulated universes look like compared to what we see. Figure 2.4 is the
272 most recent CMB image from the Plank satellite after subtracting the average value and masking the
273 galactic plane [10]. Redder regions indicate a slightly hotter region in the CMB, and blue indicates
274 colder. The intensity variations are on the order of 1 in 1000 with respect to the average value.

275 The Cosmic Microwave Background shows that the universe had DM in it from an incredibly
276 early stage. To measure the DM, Dark Energy, and matter fractions of the universe from the CMB,
277 the image is analyzed into a power spectrum, which shows the amplitude of the fluctuations as
278 a function of spherical multipole moments. Λ CDM provides the best fit to the power spectra of
279 the CMB as shown in Figure 2.5. The CMB power spectrum is quite sensitive to the fraction
280 of each energy contribution in the early universe. Low l modes are dominated by variations
281 in gravitational potential. Intermediate l emerge from oscillations in photon-baryon fluid from

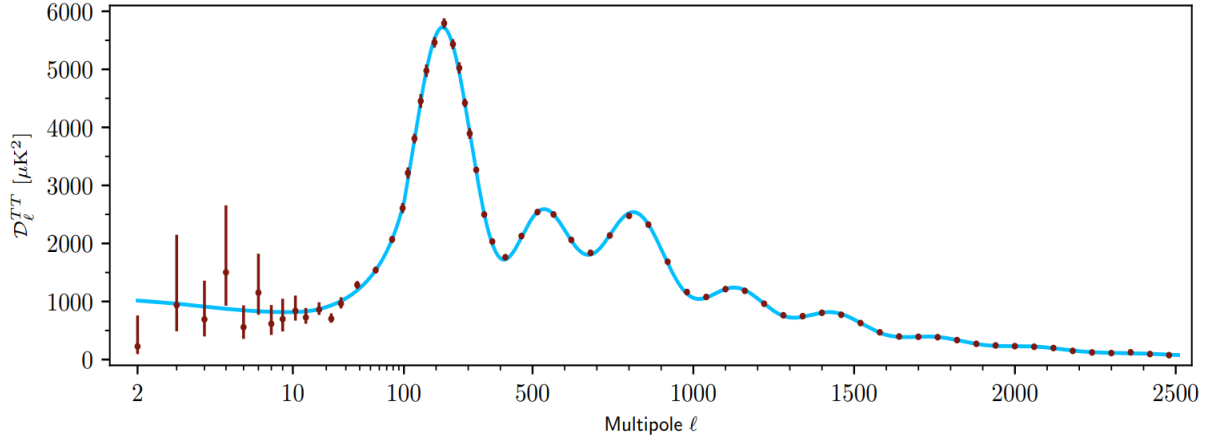


Figure 2.5 Observed Cosmic Microwave Background power spectrum as a function of multipole moment from Plank [10]. Blue line is best fit model from Λ CDM. Red points and lines are data and error, respectively.

282 competing baryon pressures and gravity. High l is a damped region from the diffusion of photons
 283 during electron-proton recombination. [1]

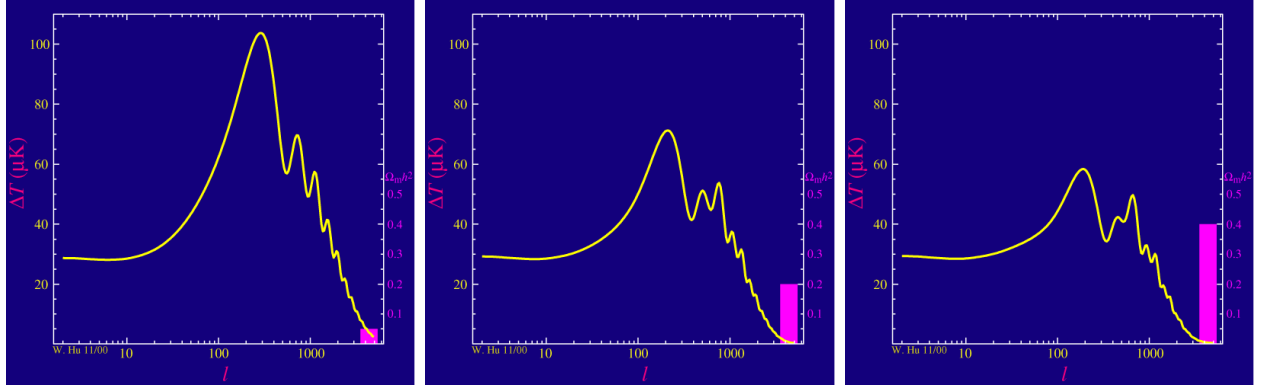


Figure 2.6 Predicted power spectra of CMB for different $\Omega_m h^2$ values for fixed baryon density from [11]. (left) Low $\Omega_m h^2$ increases the prominence of first and second peaks. (middle) $\Omega_m h^2$ is most similar to the observed power spectrum. The second and third peaks are similar in height. (right) $\Omega_m h^2$ is large which suppresses the first peak and raises the prominence of the third peak.

284 The harmonics would look quite different for a universe with less DM. Figure 2.6 demonstrates
 285 the effect $\Omega_m h^2$ has on the expected power spectrum for fixed baryon matter density. [11] Sweeping
 286 $\Omega_m h^2$ in this way clearly shows the effect dark matter has on the CMB power spectrum. The
 287 observations fit well with the Λ CDM model, and the derived fractions are as follows. The matter
 288 fraction: $\Omega_m = 0.3153$; and the baryon fraction: $\Omega_b = 0.04936$ [10]. Plank's observations also
 289 provide a measure of the Hubble constant, H_0 . H_0 especially has seen a growing tension in the

290 past decade that continues to deepened with observations from instruments like the James Webb
291 Telescope [12, 13]. As Hubble tensions deepen, we may find that perhaps Λ **CDM**, despite its
292 successes, is missing some critical physics.

293 Overall, the Newtonian motion of stars in galaxies, weak lensing from galactic clusters, and
294 power spectra from primordial light form a compelling body of research in favor of dark matter.
295 It takes another leap of theory and experimentation to make observations of DM that are non-
296 gravitational in nature. In Section 2.3, the evidence for DM implies strongly that the DM is matter
297 and not a lost parameter in the gravitational fields between massive objects. Finally, if we take one
298 axiom: that this matter has quantum behavior, such as being described by some Bohr wavelength
299 and abiding by some fermion or boson statistics; then we arrive at particle dark matter. One particle
300 DM hypothesis is the Weakly Interacting Massive Particle (WIMP). This DM candidate theory is
301 discussed further in the next section and is the focus of this thesis.

302 2.4 Searching for Dark Matter: Particle DM

303 Section 2.4 shows the Standard Model of particle physics and is currently the most accurate
304 model for the dynamics of fundamental particles like electrons and photons. The current status
305 of the SM does not have a viable DM candidate. When looking at the standard model, we can
306 immediately exclude any charged particle because charged particles interact strongly with light.
307 Specifically, this will rule out the following charged, fundamental particles: $e, \mu, \tau, W, u, d, s, c, t, b$
308 and their corresponding antiparticles. Recalling from Section 2.2 that DM must be long-lived and
309 stable over the age of the universe which excludes all SM particles with decay half-lives at or shorter
310 than the age of the universe. The lifetime constraint additionally eliminates the Z and H bosons.
311 Finally, the candidate DM needs to be somewhat massive. Recall from Section 2.2 that DM is cold
312 or not relativistic through the universe. This eliminates the remaining SM particles: $\nu_{e,\mu,\tau}, g, \gamma$ as
313 DM candidates. Because there are no DM candidates within the SM, the DM problem strongly
314 hints to physics beyond the SM (BSM).

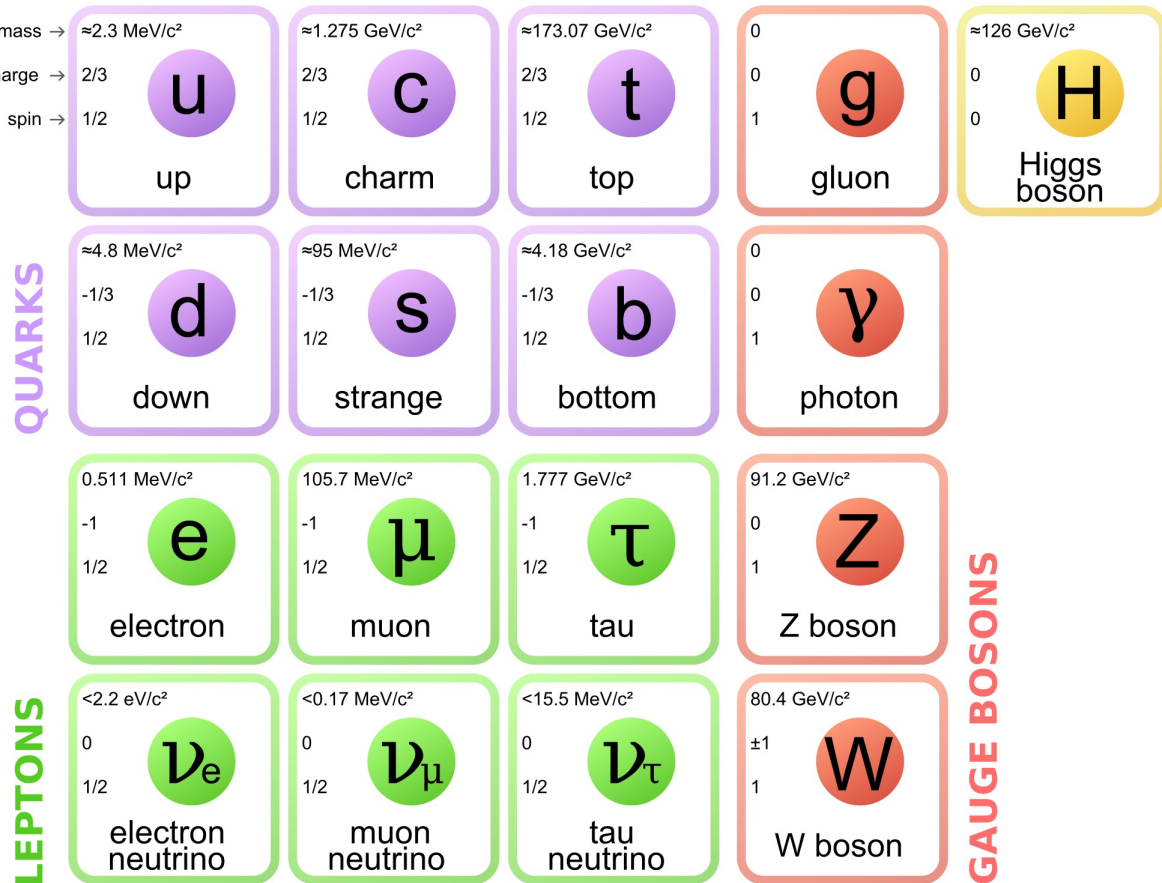


Figure 2.7 The Standard Model (SM) of particle physics. Figure taken from <http://www.quantumdiaries.org/2014/03/14/the-standard-model-a-beautiful-but-flawed-theory/>

315 2.4.1 Shake it, Break it, Make it

316 When considering DM that couples in some way with the SM, the interactions are roughly
 317 demonstrated by interaction demonstrated in Figure 2.8. The figure is a simplified Feynman
 318 diagram where the arrow of time represents the interaction modes of: **Shake it, Break it, Make it**.

319 **Shake it** refers to the direct detection of dark matter. Direct detection interactions start with
 320 a free DM particle and an SM particle. The DM and SM interact via elastic or inelastic collision
 321 and recoil away from each other. The DM remains in the dark sector and imparts some momentum
 322 onto the SM particle. The hope is that the momentum imparted onto the SM particle is sufficiently
 323 high enough to pick up with extremely sensitive instruments. Because we cannot create the DM in
 324 the lab, a direct detection experiment must wait until DM is incident on the detector. Most direct
 325 detection experiments are therefore placed in low-background environments with inert detection

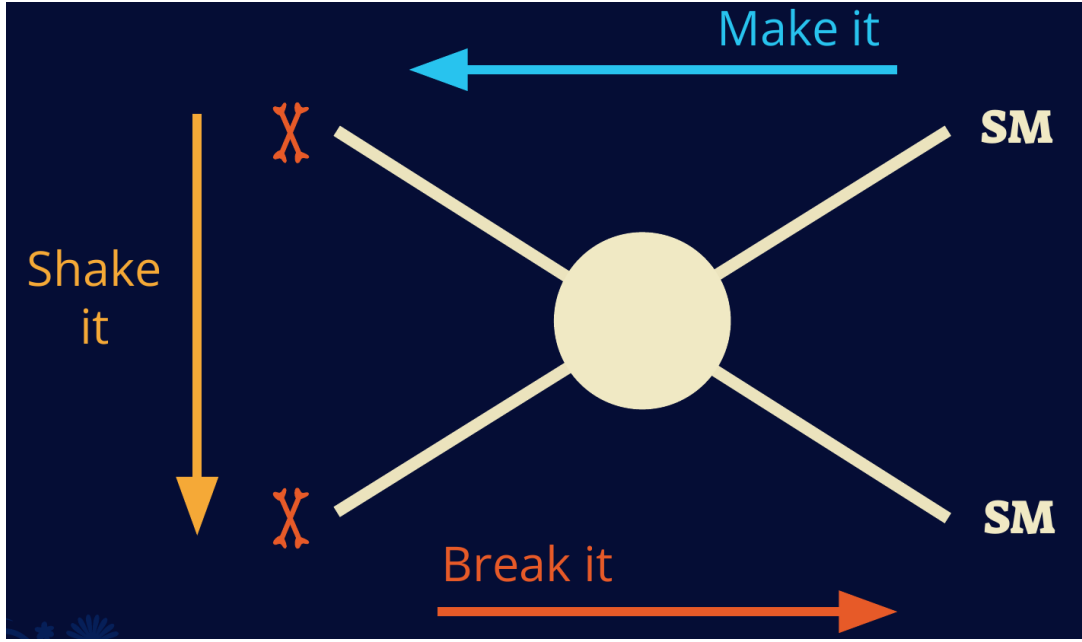


Figure 2.8 Simplified Feynman diagram demonstrating different ways DM can interact with SM particles. The 'X's refer to the DM particles whereas the SM refer to fundamental particles in the SM. The large circle in the center indicates the vertex of interaction and is purposely left vague. The colored arrows refer to different directions of time as well as their respective labels. The arrows indicate the initial and final state of the DM -SM interaction in time.

326 media like the noble gas Xenon. [14]

327 **Make it** refers to the production of DM from SM initial states. The experiment starts with
 328 particles in the SM. These SM particles are accelerated to incredibly high energies and then collide
 329 with each other. In the confluence of energy, DM hopefully emerges as a byproduct of the SM
 330 annihilation. Often it is the collider experiments that are energetic enough to hypothetically produce
 331 DM. These experiments include the world-wide collaborations ATLAS and CMS at CERN where
 332 proton collide together at extreme energies. The DM searches, however, are complex. DM likely
 333 does not interact with the detectors and lives long enough to escape the detection apparatus of
 334 CERN's colliders. This means any DM production experiment searches for an excess of events
 335 with missing momentum or energy in the events. An example event with missing transverse
 336 momentum is shown in Figure 2.9. The missing momentum with no particle tracks implies a
 337 neutral particle carried the energy out of the detector. However, there are other neutral particles
 338 in the SM, like neutrons or neutrinos, so any analysis has to account for SM signatures of missing

339 momentum. [15]

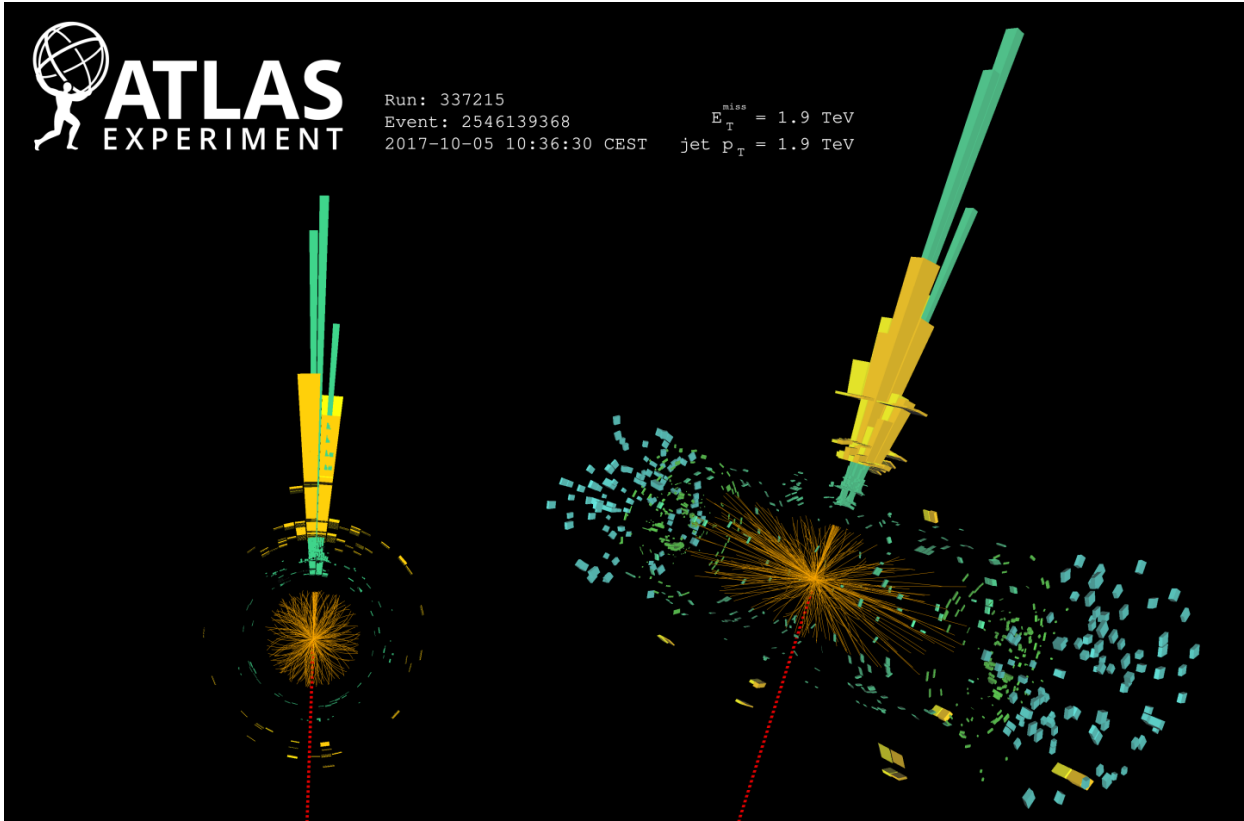


Figure 2.9 A single jet event in ATLAS detector from 2017 [16]. Jet momentum was observed to be 1.9 TeV. Missing transverse momentum was observed to be 1.9 TeV compared to the initial transverse momentum of the event was 0. Implied MET is traced by a red dashed line in event display.

340 2.4.2 Break it: Standard Model Signatures of Dark Matter through Indirect Searches

341 **Break it** refers to the creation of SM particles from the dark sector, and it is the primary focus
342 of this thesis. The interaction begins with DM or in the dark sector. The hypothesis is that this
343 DM will either annihilate with itself or decay and produce an SM byproduct. This method is
344 often referred to as the Indirect Detection of DM because we have no lab to directly control or
345 manipulate the DM. Therefore, most indirect DM searches are performed using observations of
346 known DM densities among the astrophysical sources. The strength is that we have the whole of the
347 universe and its 13.6-billion-year lifespan to use as a detector and particle accelerator. Additionally,
348 locations of dark matter are well cataloged since it was astrophysical observations that presented

349 the problem of DM in the first place.

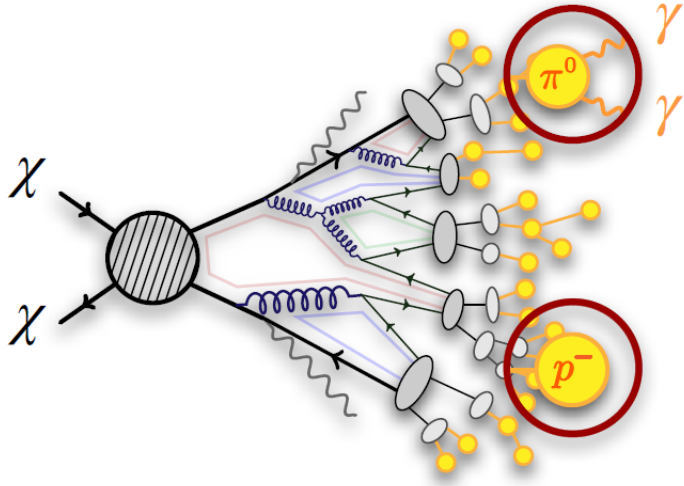


Figure 2.10 More detailed pseudo-Feynman diagram of particle cascade from dark matter annihilation into 2 quarks. The quarks hadronize and down to stable particles like γ or the anti-proton (p^-). Diagram pulled from ICRC 2021 presentation on DM annihilation search [17].

350 However, anything can happen in the universe. There are many difficult to deconvolve back-
351 grounds when searching for DM. One prominent example is the galactic center. We know the
352 galactic center has a large DM content because of stellar kinematics in our Milky Way and DM halo
353 simulations. Yet, any signal from the galactic center is challenging to parse apart from the extreme
354 environment of our supermassive black hole, unresolved sources, and diffuse emission from the
355 interstellar medium [18]. Despite the challenges, any DM model that yields evidence in the other
356 two observation methods, **Shake it or Make it** must be corroborated with indirect observations of
357 the known DM sources. Without corroborating evidence, DM observation in the lab is hard-pressed
358 to demonstrate that it is the model contributing to the DM seen at the universal scale.

359 In the case of WIMP DM, signals are described in terms of primary SM particles produced
360 from DM decay or annihilation. The SM initial state particles are then simulated down to stable
361 final states such as the γ , ν , p , or e which can traverse galactic lengths to reach Earth.

362 Figure 2.10 shows the quagmire of SM particles that emerges from SM initial states that are not
363 stable [17]. There are many SM particles with varying energies that can be produced in such an

364 interaction. For any arbitrary DM source and stable SM particle, the SM flux from DM annihilating
 365 to a neutral particle in the SM, ϕ , from a region in the sky is described by the following.

$$\frac{d\Phi_\phi}{dE_\phi} = \frac{\langle\sigma v\rangle}{8\pi m_\chi^2} \frac{dN_\phi}{dE_\phi} \times \int_{\text{source}} d\Omega \int_{l.o.s} \rho_\chi^2 dl(r, \theta') \quad (2.4)$$

366 In Equation (7.1), $\langle\sigma v\rangle$ is the velocity-weighted annihilation cross-section of DM to the SM. m_χ
 367 refers to the mass of DM, noted with Greek letter χ . $\frac{dN_\phi}{dE_\phi}$ is the N particle flux weighted by the
 368 particle energy. An example is provided in Figure 2.11 for the γ final state. The integrated terms
 369 are performed over the solid angle, $d\Omega$, and line of sight, l.o.s. ρ is the density of DM for a
 370 location (r, θ') in the sky. The terms left of the '×' are often referred to as the particle physics
 371 component. The terms on the right are referred to as the astrophysical component. For decaying
 372 DM, the equation changes to...

$$\frac{d\Phi_\phi}{dE_\phi} = \frac{1}{4\pi\tau m_\chi} \frac{dN_\phi}{dE_\phi} \times \int_{\text{source}} d\Omega \int_{l.o.s} \rho_\chi dl(r, \theta') \quad (2.5)$$

373 In Equation (2.5), τ is the decay lifetime of the DM. Just as in Equation (7.1), the left and
 374 right terms are the particle physics and the astrophysical components respectively. The integrated
 375 astrophysical component of Equation (7.1) is often called the J-Factor. Whereas the integrated
 376 astrophysical component of Equation (2.5) is often called the D-Factor.

377 Exact DM $\text{DM} \rightarrow \text{SM SM}$ branching ratios are not known, so it is usually assumed to go 100%
 378 into an SM particle/anti-particle. Additionally, when a DM annihilation or decay produces one of
 379 the neutral, long-lived SM particles (ν or γ), the particle is traced back to a DM source. For DM
 380 above GeV energies, there are very few SM processes that can produce particles with such a high
 381 energy. Seeing such a signal would almost certainly be an indication of the presence of dark matter.
 382 Fortunately, the universe provides us with the largest volume and lifetime ever for a particle physics
 383 experiment.

384 2.5 Sources for Indirect Dark Matter Searches

385 The first detection of DM relied on optical observations. Since then, we have developed new
 386 techniques to find DM dense regions. As described in Section 2.3.1, many DM dense regions were
 387 through observing galactic rotation curves. Our Milky Way galaxy is among DM dense regions

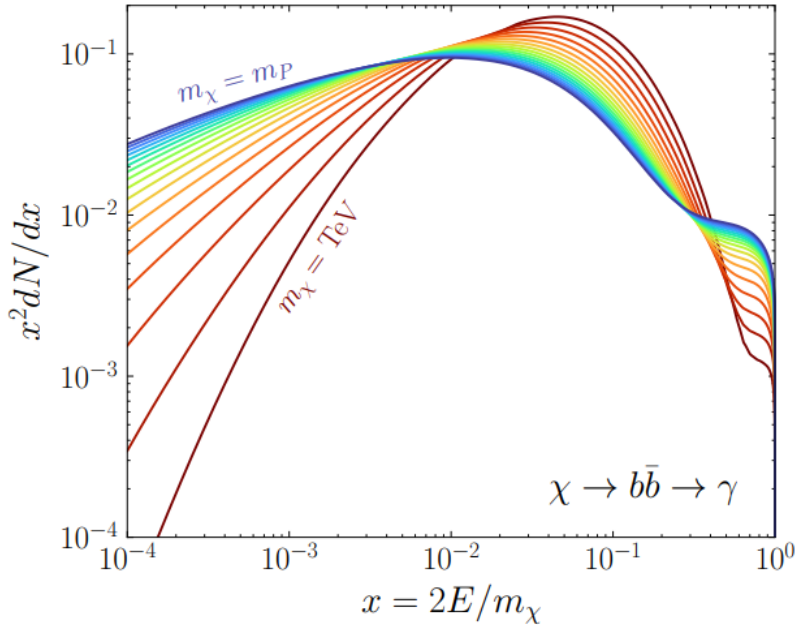


Figure 2.11 Dark Matter (DM) decay spectrum for $b\bar{b}$ initial state and γ final state. Redder spectra are for larger DM masses. Bluer spectra are light DM masses. x is a unitless factor defined as the ratio of the mass of DM, m_χ , and the final state particle energy E_γ . Figure from [19].

discovered, and it is the largest nearby DM dense region to look at. Additionally, the DM halo surrounding the Milky Way is clumpy [18]. There are regions in the DM halo of the Milky Way that have more DM than others that have captured gas over time. These sub-halos were dense enough collapse gas and form stars. These apparent sub galaxies are known as dwarf spheroidal galaxies and are the main sources studied in this thesis. Each source type comes with different trade-offs. Galactic Center studies will be very sensitive to the assumed distribution of DM. The central DM density can vary substantially as demonstrated in Figure 2.12. At distances close to the center of the galaxy, or small r , the differences in DM densities can be 3-4 orders of magnitude. Searches toward the galactic center will therefore be quite sensitive to the assumed DM distribution.

Searches toward Dwarf Spheroidal Galaxies (dSph's) suffer from uncertainties in the DM density less than the galactic center studies. This is mostly from their diminutive size being smaller than the angular resolution of most γ -ray observatories [18]. The DM content dSph's are typically determined with the Virial theorem, Equation (2.1), and are usually majority DM [18] in mass. DSph's tend to be ideal sources to look at for DM searches. Their environments are quiet with little

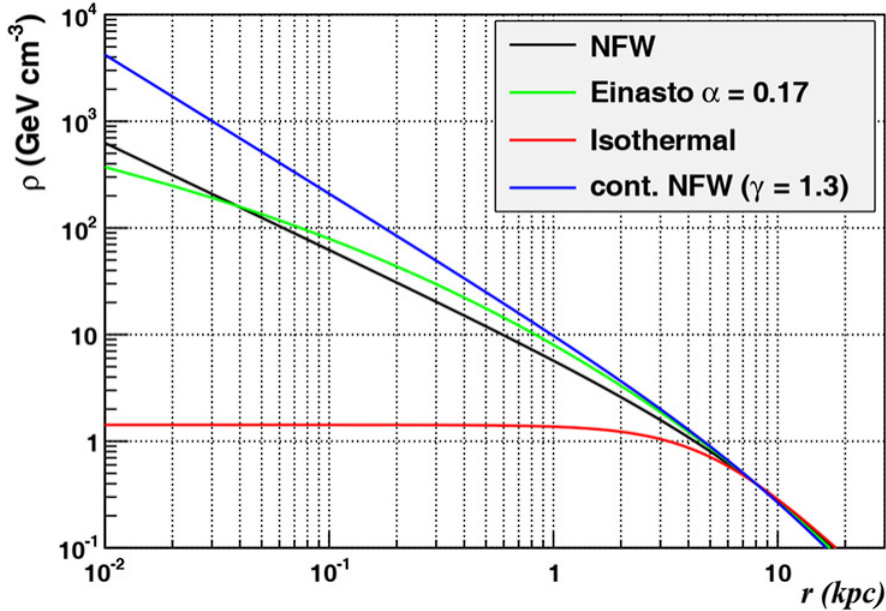


Figure 2.12 Different dark matter density profiles compared. Some models produce exceptionally large densities at small r [20].

402 astrophysical background. Unlike the galactic center, the most active components of dSph's are the
 403 stars within them versus a violent accretion disc around a black hole. All this together means that
 404 dSph's are among the best sources to look at for indirect DM searches. dSph's are the targets of
 405 focus for this thesis.

406 2.6 Multi-Messenger Dark Matter

407 Astrophysics entered a new phase in the past few decades that leverages our increasing sensitivity
 408 to SM channels and general relativity (GR). Up until the 21st century, astrophysical observations
 409 were performed with photons (γ) only. Astrophysics with this 'messenger' is fairly mature now.
 410 Novel observations of the universe have since only adjusted the sensitivity of the wavelength of
 411 light that is observed except at MeV energies. Gems like the CMB [10], and more have ultimately
 412 been observations of different wavelengths of light. Multi-messenger astrophysics proposes using
 413 other SM particles such the p^{+-} , or ν or gravitation waves predicted by general relativity.

414 The experiment LIGO had a revolutionary discovery in 2016 with the first detection of a binary
 415 black hole merger [21]. This opened the collective imagination to observing the universe through
 416 gravitational waves. There has also been a surge of interest in the neutrino (ν) sector. IceCube

417 demonstrated that we are sensitive to neutrinos in regions that correlate with significant photon
 418 emission like the galactic plane [22]. Neutrinos, like gravitational waves and light, travel mostly
 419 unimpeded from their source to our observatories. This makes pointing to the originating source
 420 of these messengers much easier than it is for cosmic rays which are deflected from their source by
 421 magnetic fields.

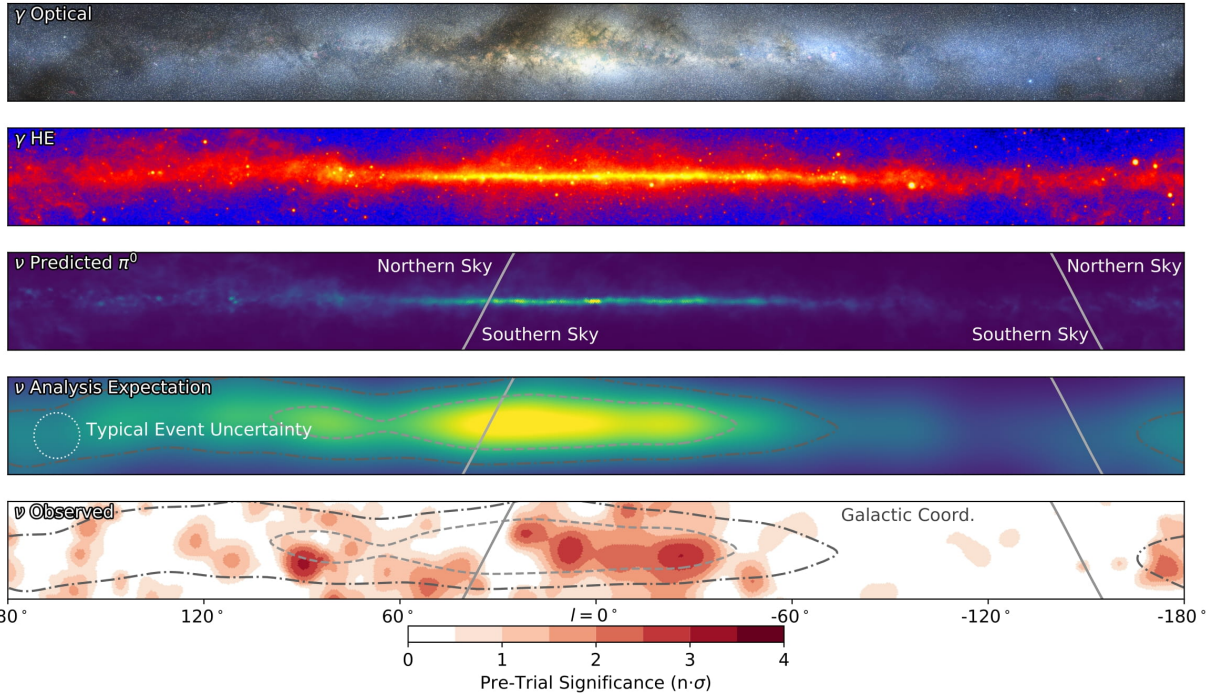


Figure 2.13 The Milky Way Galaxy in photons (γ) and neutrinos (ν) [22]. The Galactic center is at $l=0^\circ$ and is the brightest region in all panels. (top) An Optical color image of the Milky Way galaxy seen from Earth. Clouds of gas and dust obscure some light from stars. (2nd down) Integrated flux of γ -rays observed by the Fermi-LAT telescope [23]. (middle) Expected neutrino emission that corresponds with Fermi-LAT observations. (2nd up) Expected neutrino emission profile after considering detector systematics of IceCube. (bottom) Observed neutrino emission from region of the galactic plane. Substantial neutrino emission was detected.

422 The IceCube collaboration recently published a groundbreaking result of the Milky Way in
 423 neutrinos. The recent result from IceCube, shown in Figure 2.13, proves that we can make
 424 observations under different messenger regimes. The top two panels show the appearance of the
 425 galactic plane to different wavelengths of light. Some sources are more apparent in some panels,
 426 while others are not. This new channel is powerful because neutrinos are readily able to penetrate
 427 through gas and dust in the Milky Way. This new image also refines our understanding of how high

428 energy particles are produced. For example, the fit to IceCube data prefers neutrino production
 429 from the decay of π^0 [22].

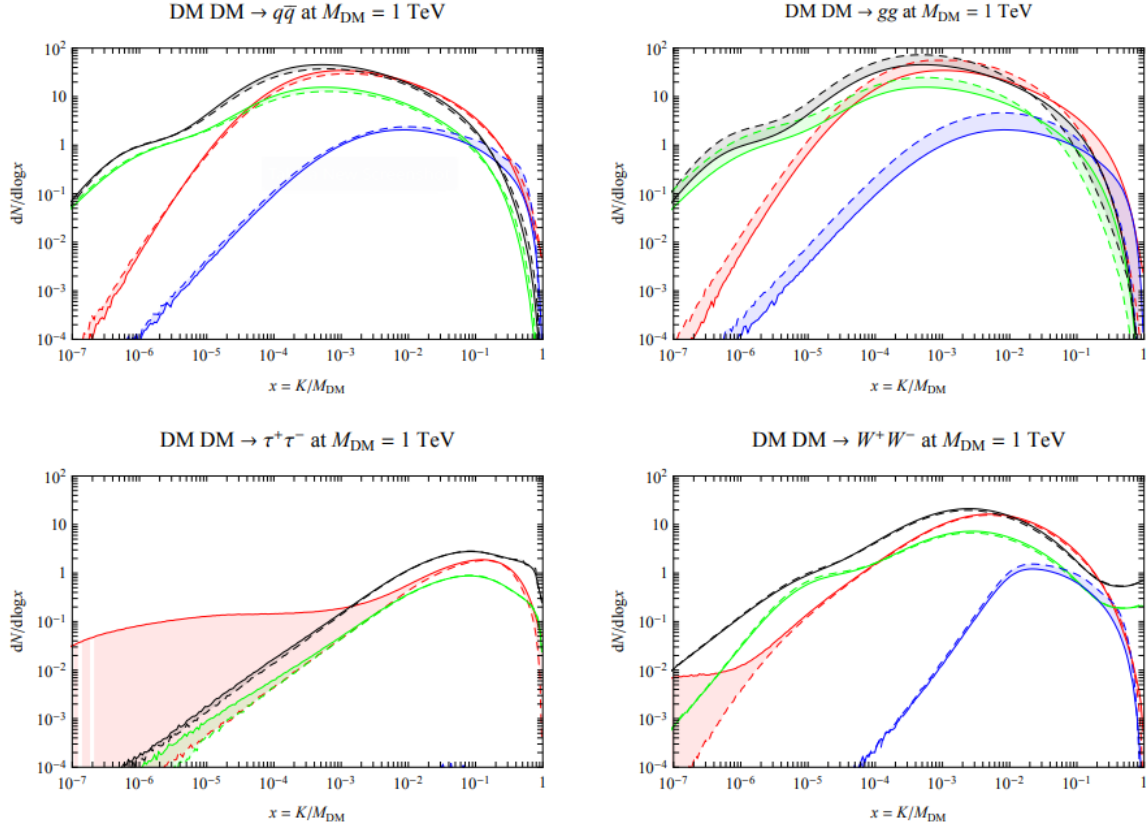


Figure 2.14 Dark Matter annihilation spectra for different final state particle and standard model annihilation channels [24]. Photons (red), e^\pm (green), \bar{p} (blue), ν (black).

430 Exposing our observations to more cosmic messengers greatly increases our sensitivity to
 431 rare processes. In the case of DM, Figure 2.14, there are many SM particles produced in DM
 432 annihilation. Among the final state fluxes are gammas and neutrinos. Charged particles are also
 433 produced however they would not likely make it to Earth since they will be deflected by magnetic
 434 fields between the source and Earth. This means observatories that can see the neutral messengers
 435 are especially good for DM searches and for combining data for a multi-messenger DM search.

CHAPTER 3

436 MULTIMESSENGER ASTROPHYSICS: DETECTING HIGH ENERGY NEUTRAL 437 MESSENGERS

438 3.1 Introduction

439 Before the 20th century, all asttrophysics observations were optical in nature. We litterly only
440 saw things with highly magnified optical observations. Then we discovered cosmic rays. cosmic
441 rays are charged particles, typically naked protons or H+. This was seen by Victor Hess in 19??.
442 Around the same time we discovered neutrinos from beta decay. Sometime around 1950 we started
443 to build neutrino detectors which were mostly sensitive to neutrinos from the sun. Finally, it was
444 theorized that compact objects like black holes and neutron stars would create waves in space-time
445 when they experience mergers or collisions.

446 In the 21st century, we have developed new observation techniques and detectors that are no only
447 sensitive to these four messengers - photons (TODO: photon), neutrinos (TODO: nu), Cosmic
448 Rays (CR), and Gravitational Wave (WV) - we're collect high energy versions of these events.
449 For the standad model particles, we're now sensitive to all messengers above the MeV eneryg
450 range. Additionally, the GW's were sensitive to are in the stellar mass black hole region and above
451 within our galactic neighborhood. This means were becoming sensitive to the fundamental physics
452 occuring within the universe and we can rely on the universe as a TeV+ particle accelerator. We
453 also have the abaility to correlate high energy events across messengers and gain new insights on
454 the processes that occur in our universe.

455 This thesis focuses on very high energy (VHE) gamma rays and neutrinos. These can both be
456 observed through the water cherenkov detection technique altho not exclusively. Methods on how
457 to detect and observe these neutral messengers are discussed Section 3.3 and Section 3.4

458 3.2 Charged Particles in a Medium

459 For high enery gamma-rays and neutrinos, we can exploit the same effect that charged particles
460 have with water. This effect is known as Cherenkov radiation. Cherenkov Radiation occurs when a
461 charged particle, usually electrons (e) or muons (μ), traverse a medium, like water, faster than the

462 speed of light in that medium. This is similar to sonic boom where an object moves through air
463 faster than the speed of sound in air. Cherenkov radiation can therefore be thought of as an 'optic
464 boom'. Many astro-particle physics experiments will use water as the medium as because water
465 has a unique set of properties ideal for charged particle tracking.



Figure 3.1 TODO: Show a nuclear reactor with cherenkov radiation[NEEDS A SOURCE][FACT CHECK THIS]

466 The frequency of light emitted due to cherenkov radiation follows the equation:

$$INSERT\ Cherenkov\ wavelength\ calc\ HERE. \quad (3.1)$$

467 The absorption spectra is shown in the following figure:

468 **3.3 Photons (γ)**

469 **3.4 Neutrinos (ν)**

470 **3.5 Opportunities to Combine for Dark Matter**



Figure 3.2 TODO: absorption spectrum of liquid and solid water[NEEDS A SOURCE][FACT CHECK THIS]

CHAPTER 4

471

HIGH ALTITUDE WATER CHERENKOV (HAWC) OBSERVATORY

472 **4.1 The Detector**

473 **4.2 Events Reconstruction and Data Acquisition**

474 **4.2.1 G/H Discrimination**

475 **4.2.2 Angle**

476 **4.2.3 Energy**

477 **4.3 Remote Monitoring**

478 **4.3.1 ATHENA Database**

479 **4.3.2 HOMER**

480

CHAPTER 5

ICECUBE NEUTRINO OBSERVATORY

481 **5.1 The Detector**

482 **5.2 Events Reconstruction and Data Acquisition**

483 **5.2.1 Angle**

484 **5.2.2 Energy**

485 **5.3 Northern Test Site**

486 **5.3.1 PIgeon remote dark rate testing**

487 **5.3.2 Bulkhead Construction**

CHAPTER 6

COMPUTATIONAL TECHNIQUES IN PARTICLE ASTROPHYSICS

489 **6.1 Neural Networks for Gamma/Hadron Separation**

490 **6.2 Parallel Computing for Dark Matter Analyses**

491

CHAPTER 7

GLORY DUCK

492 **7.1 Dataset and Background**493 **7.1.1 Data Files**

- 494 • Detector Resolution: `response_aerie_svn_27754_systematics_best_mc_test_no`
 495 `broadpulse_10pctlogchargesmearing_0.63qe_25kHzNoise_run5481_curvatu`
 496 `re0_index3.root`
- 497 • Data Map: `maps-20180119/liff/maptree_1024.root`

498 **7.1.2 Data Set Chosen**

499 The maps used for this analysis contain 1017 days of data between runs 2104 (2014-11-26) and
 500 7476 (2017-12-20). They were generated from pass 4.0 reconstruction. The analysis is performed
 501 using the f_{hit} energy binning scheme with bins [1-9] similar to what was done for the Crab and
 502 previous HAWC dSph analysis. [25, 26].

503 **7.1.3 Background Estimation**

504 This analysis was done on dwarf spheroidal (dSph) galaxies because of their large dark matter
 505 (DM) content relative to baryonic. We consider the following to estimate the background to this
 506 study.

- 507 • The dSphs are small in HAWC's field of view, so the analysis is not sensitive to large or small
 508 scale anisotropies.
- 509 • The dSphs used in this analysis are off the galactic plane.
- 510 • The dSphs are baryonically faint relative to their expected dark matter content and are not
 511 expected to contain gamma-ray sources.

512 Therefor we make no additional assumptions of the background coming from our sources and
 513 use HAWC's standard direct integration method for background estimation. It is possible for gamma

514 rays from DM annihilation to scatter in transit to HAWC via Inverse Compton Scattering (ICS).
515 This was investigated and its impact on the flux is basically zero. Supporting information on this
516 is in **TODO: refer to appdx**

517 **7.1.4 Software Tools and Development**

518 This analysis was performed using HAL and 3ML, in Python version 2.[25, 27] Dan developed
519 a source model to implement the *Poor Particle Physicists' Cookbook* (PPPC) [28] into HAWC
520 software. This model and corresponding Monte Carlo simulation was consolidated into a dictionary
521 for other collaborators. A NumPy version of this dictionary was made for both Py2 and Py3. The
522 code base for creating this dictionary is also in Dan's sandbox:

- 523 • Py2: <https://gitlab.com/hawc-observatory/sandboxes/salaza82/glory-duc>
524 k-hawc/-/tree/master/GD_spectrumDictionary Generator (Deprecated)
- 525 • Py3: <https://gitlab.com/hawc-observatory/sandboxes/salaza82/pppc2dictPPPC2Dict>

527 The analysis was performed using the f_{hit} framework performed in the Crab paper[25]. The
528 PPPC model selected for this analysis included electroweak corrections. Dictionaries for the
529 non-electroweak model were generated but not used for this analysis. The Python2 NumPy dictio-
530 nary file for gamma-ray final states is `dmCirSpecDict.npy`. The corresponding Python3 file is
531 `DM_CirrelliSpectrum_dict_gammas.npy`. These files can also be used for decay channels and
532 the PPPC describes how. [28]. Python's pickle is not backwards compatible, so scripts run in Py3
533 are not able to use dictionaries generated using Py2 and vice-versa.

534 All other software used for data analysis, DM profile generation, and job submission to SLURM
535 are also kept in my sandbox for <https://gitlab.com/hawc-observatory/sandboxes/sal>
536 aza82/glory-duck-hawc the Glory Duck project. They're broad descriptions are as follows:

- 537 • `GD_mass_profiles`: scripts that generate .fits maps for HAWC HAL according to [29].
538 Also contains simple plots of these maps.

- 539 • `GD_spectrum`: scripts that generate NumPy dictionaries of PPPC gamma spectra [28].
- 540 • `analysis_scripts`: HAL scripts for performing likelihood computation on HAWC data or
541 simulation with GD spectra and mass profiles.
- 542 • `pointing`: HAL scripts used to compare the impact of point systematic.
- 543 • `poisson_maps`: scripts for generating and managing poisson trials used for this study.

544 **7.2 Analysis**

545 **7.2.1 Monte Carlo Simulation**

546 The expected differential photon flux from a DM-DM annihilation to standard model particles
547 over solid angle is described by the familiar equation.

$$\frac{d\Phi_\gamma}{dE_\gamma} = \frac{\langle\sigma v\rangle}{8\pi m_\chi^2} \frac{dN_\gamma}{dE_\gamma} \times \int_{\text{source}} d\Omega \int_{l.o.s} \rho_\chi^2 dl(r, \theta') \quad (7.1)$$

548 Where $\langle\sigma v\rangle$ is the velocity weighted annihilation cross-section. $\frac{dN}{dE}$ is the expected differential
549 number of photons produced at each energy per annihilation. M_χ is the rest mass of the supposed
550 DM particle. J is the astrophysical J-factor and is defined as

551 ρ_χ is the DM density. For this value, we import the PPPC with electroweak corrections [28].
552 The spectrum is implemented as a model script in astromodels for 3ML. The J-factor profiles for
553 each source is imported from Geringer-Sameth (\mathcal{GS}) [30]. Another DM distribution model from
554 Bonnivard (\mathcal{B}) [31] was used for the complete study. However, to save computational time, limits
555 from \mathcal{GS} were scaled to \mathcal{B} instead of each experiment performing a full study a second time. We
556 create NSIDE 16384 maps of the J-factors for each dSph. These maps are integrated over every
557 spatial bin and passed to the fitting software. Plots of these maps are provided for each source in
558 the sandbox directory: `GD_mass_profiles`.

559 **7.2.2 Source Selection and Annihilation Channels**

560 We use many of the dSph presented in our previous dSph DM search [26]. HAWC's sources
561 for Glory Duck include Boötes I, Coma Berenices, Canes Venatici I + II, Draco, Hercules, Leo I,

562 II, + IV, Segue 1, Sextans, and Ursa Major I + II. A full description of all sources used in Glory
 563 Duck is found in Table 7.1. Triangulum II was excluded from the Glory Duck analysis because
 564 of large uncertainties in its J-factor. Ursa Minor was excluded from HAWC’s contribution to the
 565 combination because the source extension model extended Ursa Minor beyond HAWC’s field of
 566 view. Ursa Minor was not expected to contribute significantly to the combined limit, so work was
 567 not invested in a solution to include Ursa Minor.

568 The DM annihilation channels probed for the Glory Duck combination include $b\bar{b}$, $e\bar{e}$, $\mu\bar{\mu}$, $\tau\bar{\tau}$, $t\bar{t}$, W^+W^- , and ZZ .
 569 A summary of all sources, with a description of each experiments’ sensitivity to the source, is pro-
 570 vided in Table 7.2.

571 **7.2.3 Likelihood Methods**

572 We perform a standard HAWC binned maximum likelihood analysis using f_{hit} bins 1-9. This
 573 analysis was performed using HAL and 3ML, in Python2.[25, 27] With these tools we compute
 574 the max from the likelihood profiles and perform a ratio test to calculate the significance of each
 575 source. This analysis is identical to the previous dSph analysis [26] except the sources are treated
 576 as extended. For the vast majority of our sources, this extension is no greater than 2 degrees. We
 577 calculate the likelihood of each source and model, assuming events are Poisson distributed, with

$$\mathcal{L} = \prod_i \frac{(B_i + S_i)^{N_i} e^{-(B_i + S_i)}}{N_i!} \quad (7.2)$$

578 S_i is the sum of expected number of signal counts. B_i is the number of background counts
 579 observed. N_i is the total number of counts. The i th bin is iterated over spatial and f_{hit} . Then we
 580 combine the profiles across all five experiments. The profile likelihood ratio λ as a function of
 581 annihilation cross-section $\langle\sigma v\rangle$ is computed by:

$$\lambda(\langle\sigma v\rangle | \mathcal{D}_{\text{dSphs}}) = \frac{\mathcal{L}(\langle\sigma v\rangle; \hat{\nu} | \mathcal{D}_{\text{dSphs}})}{\mathcal{L}(\widehat{\langle\sigma v\rangle}; \hat{\nu} | \mathcal{D}_{\text{dSphs}})} \quad (7.3)$$

Table 7.1 Summary of the relevant properties of the dSphs used in the present work. Column 1 lists the dSphs. Columns 2 and 3 present their heliocentric distance and galactic coordinates, respectively. Columns 4 and 5 report the J -factors of each source given from the \mathcal{GS} and \mathcal{B} independent studies and their estimated $\pm 1\sigma$ uncertainties. The values $\log_{10} J$ (\mathcal{GS} set) [30] correspond to the mean J -factor values for a source extension truncated at the outermost observed star. The values $\log_{10} J$ (\mathcal{B} set) [31] are provided for a source extension at the tidal radius of each dSph. **Bolded sources are within HAWC's field of view and provided to the Glory Duck analysis.**

Name	Distance (kpc)	l, b ($^{\circ}$)	$\log_{10} J$ (\mathcal{GS} set) $\log_{10}(\text{GeV}^2\text{cm}^{-5}\text{sr})$	$\log_{10} J$ (\mathcal{B} set) $\log_{10}(\text{GeV}^2\text{cm}^{-5}\text{sr})$
Boötes I	66	358.08, 69.62	$18.24^{+0.40}_{-0.37}$	$18.85^{+1.10}_{-0.61}$
Canes Venatici I	218	74.31, 79.82	$17.44^{+0.37}_{-0.28}$	$17.63^{+0.50}_{-0.20}$
Canes Venatici II	160	113.58, 82.70	$17.65^{+0.45}_{-0.43}$	$18.67^{+1.54}_{-0.97}$
Carina	105	260.11, -22.22	$17.92^{+0.19}_{-0.11}$	$18.02^{+0.36}_{-0.15}$
Coma Berenices	44	241.89, 83.61	$19.02^{+0.37}_{-0.41}$	$20.13^{+1.56}_{-1.08}$
Draco	76	86.37, 34.72	$19.05^{+0.22}_{-0.21}$	$19.42^{+0.92}_{-0.47}$
Fornax	147	237.10, -65.65	$17.84^{+0.11}_{-0.06}$	$17.85^{+0.11}_{-0.08}$
Hercules	132	28.73, 36.87	$16.86^{+0.74}_{-0.68}$	$17.70^{+1.08}_{-0.73}$
Leo I	254	225.99, 49.11	$17.84^{+0.20}_{-0.16}$	$17.93^{+0.65}_{-0.25}$
Leo II	233	220.17, 67.23	$17.97^{+0.20}_{-0.18}$	$18.11^{+0.71}_{-0.25}$
Leo IV	154	265.44, 56.51	$16.32^{+1.06}_{-1.70}$	$16.36^{+1.44}_{-1.65}$
Leo V	178	261.86, 58.54	$16.37^{+0.94}_{-0.87}$	$16.30^{+1.33}_{-1.16}$
Leo T	417	214.85, 43.66	$17.11^{+0.44}_{-0.39}$	$17.67^{+1.01}_{-0.56}$
Sculptor	86	287.53, -83.16	$18.57^{+0.07}_{-0.05}$	$18.63^{+0.14}_{-0.08}$
Segue I	23	220.48, 50.43	$19.36^{+0.32}_{-0.35}$	$17.52^{+2.54}_{-2.65}$
Segue II	35	149.43, -38.14	$16.21^{+1.06}_{-0.98}$	$19.50^{+1.82}_{-1.48}$
Sextans	86	243.50, 42.27	$17.92^{+0.35}_{-0.29}$	$18.04^{+0.50}_{-0.28}$
Ursa Major I	97	159.43, 54.41	$17.87^{+0.56}_{-0.33}$	$18.84^{+0.97}_{-0.43}$
Ursa Major II	32	152.46, 37.44	$19.42^{+0.44}_{-0.42}$	$20.60^{+1.46}_{-0.95}$
Ursa Minor	76	104.97, 44.80	$18.95^{+0.26}_{-0.18}$	$19.08^{+0.21}_{-0.13}$

Table 7.2 Summary of dSph observations by each experiment used in this work. A ‘-’ indicates the experiment did not observe the dSph for this study. For Fermi-LAT, the exposure at 1 GeV is given. For HAWC, $|\Delta\theta|$ is the absolute difference between the source declination and HAWC latitude. HAWC is more sensitive to sources with smaller $|\Delta\theta|$. For IACTs, we show the zenith angle range, the total exposure, the energy range, the angular radius θ of the signal or ON region, the ratio of exposures between the background-control (OFF) and signal (ON) regions (τ), and the significance of gamma-ray excess in standard deviations, σ .

Source name	Fermi-LAT	HAWC	H.E.S.S, MAGIC, VERITAS						
	Exposure (10^{11} s m 2)	$ \Delta\theta $ (°)	IACT	Zenith (°)	Exposure (h)	Energy range (GeV)	θ (°)	τ	S (σ)
Boötes I	2.6	4.5	VERITAS	15 – 30	14.0	100–41000	0.10	8.6	-1.0
Canes Venatici I	2.9	14.6	–	–	–	–	–	–	–
Canes Venatici II	2.9	15.3	–	–	–	–	–	–	–
Carina	3.1	–	H.E.S.S.	27 – 46	23.7	310 – 70000	0.10	18.0	-0.3
Coma Berenices	2.7	4.9	H.E.S.S.	47 – 49	11.4	550 – 70000	0.10	14.4	-0.4
			MAGIC	5 – 37	49.5	60 – 10000	0.17	1.0	–
			MAGIC	29 – 45	52.1	70 – 10000	0.22	1.0	–
Draco	3.8	38.1	VERITAS	25 – 40	49.8	120 – 70000	0.10	9.0	-1.0
Fornax	2.7	–	H.E.S.S.	11 – 25	6.8	230 – 70000	0.10	45.5	-1.5
Hercules	2.8	6.3	–	–	–	–	–	–	–
Leo I	2.5	6.7	–	–	–	–	–	–	–
Leo II	2.6	3.1	–	–	–	–	–	–	–
Leo IV	2.4	19.5	–	–	–	–	–	–	–
Leo V	2.4	–	–	–	–	–	–	–	–
Leo T	2.6	–	–	–	–	–	–	–	–
Sculptor	2.7	–	H.E.S.S.	10 – 46	11.8	200 – 70000	0.10	19.8	-2.2
Segue I	2.5	2.9	MAGIC	13 – 37	158.0	60 – 10000	0.12	1.0	-0.5
			VERITAS	15 – 35	92.0	80 – 50000	0.10	7.6	0.7
Segue II	2.7	–	–	–	–	–	–	–	–
Sextans	2.4	20.6	–	–	–	–	–	–	–
Ursa Major I	3.4	32.9	–	–	–	–	–	–	–
Ursa Major II	4.0	44.1	MAGIC	35 – 45	94.8	120 – 10000	0.30	1.0	-2.1
Ursa Minor	4.1	–	VERITAS	35 – 45	60.4	160 – 93000	0.10	8.4	-0.1

CHAPTER 8

NU DUCK

582

BIBLIOGRAPHY

- 584 [1] Anne M. Green. “Dark matter in astrophysics/cosmology”. In: *SciPost Phys. Lect.*
 585 *Notes* (2022), p. 37. doi: [10.21468/SciPostPhysLectNotes.37](https://doi.org/10.21468/SciPostPhysLectNotes.37). URL: <https://scipost.org/10.21468/SciPostPhysLectNotes.37>.
- 587 [2] Bing-Lin Young. “A survey of dark matter and related topics in cosmology”. In: *Frontiers*
 588 *of Physics* 12 (Oct. 2016). doi: <https://doi.org/10.1007/s11467-016-0583-4>.
 589 URL: <https://doi.org/10.1007/s11467-016-0583-4>.
- 590 [3] Gianfranco Bertone, Dan Hooper, and Joseph Silk. “Particle dark matter: evidence,
 591 candidates and constraints”. In: *Physics Reports* 405.5 (2005), pp. 279–390. ISSN:
 592 0370-1573. doi: <https://doi.org/10.1016/j.physrep.2004.08.031>. URL:
 593 <https://www.sciencedirect.com/science/article/pii/S0370157304003515>.
- 594 [4] Gianfranco Bertone and Dan Hooper. “History of dark matter”. In: *Rev. Mod. Phys.*
 595 90 (4 Aug. 2018), p. 045002. doi: [10.1103/RevModPhys.90.045002](https://doi.org/10.1103/RevModPhys.90.045002). URL: <https://link.aps.org/doi/10.1103/RevModPhys.90.045002>.
- 597 [5] Fritz Zwicky. “The Redshift of Extragalactic Nebulae”. In: *Helvetica Physica Acta* 6.
 598 (1933), pp. 110–127. doi: [10.5169/seals-110267](https://doi.org/10.5169/seals-110267).
- 599 [6] Vera C. Rubin and Jr. Ford W. Kent. “Rotation of the Andromeda Nebula from a Spectro-
 600scopic Survey of Emission Regions”. In: *ApJ* 159 (Feb. 1970), p. 379. doi: [10.1086/150317](https://doi.org/10.1086/150317).
- 602 [7] K. G. Begeman, A. H. Broeils, and R. H. Sanders. “Extended rotation curves of spiral galax-
 603 ies: dark haloes and modified dynamics”. In: *Monthly Notices of the Royal Astronomical So-*
 604 *ciety* 249.3 (Apr. 1991), pp. 523–537. ISSN: 0035-8711. doi: [10.1093/mnras/249.3.523](https://doi.org/10.1093/mnras/249.3.523).
 605 eprint: <https://academic.oup.com/mnras/article-pdf/249/3/523/18160929/mnras249-0523.pdf>. URL: <https://doi.org/10.1093/mnras/249.3.523>.
- 607 [8] *Different types of gravitational lenses*. website. Feb. 2004. URL: <https://esahubble.org/images/heic0404b/>.
- 609 [9] Douglas Clowe et al. “A Direct Empirical Proof of the Existence of Dark Matter”. In: *apjl*
 610 648.2 (Sept. 2006), pp. L109–L113. doi: [10.1086/508162](https://doi.org/10.1086/508162). arXiv: [astro-ph/0608407](https://arxiv.org/abs/astro-ph/0608407)
 611 [*astro-ph*].
- 612 [10] Planck Collaboration and N. et. al. Aghanim. “Planck 2018 results I. Overview and the
 613 cosmological legacy of Planck”. In: *A&A* 641 (2020). doi: [10.1051/0004-6361/201833880](https://doi.org/10.1051/0004-6361/201833880). URL: <https://doi.org/10.1051/0004-6361/201833880>.
- 615 [11] Wayne Hu. *Matter Density Animation*. web. 2024. URL: <http://background.uchicago.edu/~whu/animbut/anim2.html>.

- 617 [12] Wenlong Yuan et al. “A First Look at Cepheids in a Type Ia Supernova Host with JWST”. in:
618 *The Astrophysical Journal Letters* 940.1 (Nov. 2022). doi: [10.3847/2041-8213/ac9b27](https://doi.org/10.3847/2041-8213/ac9b27).
619 URL: <https://dx.doi.org/10.3847/2041-8213/ac9b27>.
- 620 [13] Wendy L. Freedman. “Measurements of the Hubble Constant: Tensions in Perspective”. In:
621 *The Astrophysical Journal* 919.1 (Sept. 2021), p. 16. doi: [10.3847/1538-4357/ac0e95](https://doi.org/10.3847/1538-4357/ac0e95).
622 URL: <https://dx.doi.org/10.3847/1538-4357/ac0e95>.
- 623 [14] Jodi Cooley. “Dark Matter direct detection of classical WIMPs”. In: *SciPost Phys. Lect.*
624 *Notes* (2022), p. 55. doi: [10.21468/SciPostPhysLectNotes.55](https://doi.org/10.21468/SciPostPhysLectNotes.55). URL: <https://scipost.org/10.21468/SciPostPhysLectNotes.55>.
- 626 [15] “Search for new phenomena in events with an energetic jet and missing transverse momentum
627 in pp collisions at $\sqrt{s} = 13$ TeV with the ATLAS detector”. In: *Phys. Rev. D* 103
628 (11 July 2021), p. 112006. doi: [10.1103/PhysRevD.103.112006](https://doi.org/10.1103/PhysRevD.103.112006). URL: <https://link.aps.org/doi/10.1103/PhysRevD.103.112006>.
- 630 [16] *Jetting into the dark side: a precision search for dark matter*. website. July 2020. URL:
631 <https://atlas.cern/updates/briefing/precision-search-dark-matter>.
- 632 [17] Celine Armand et. al. “Combined dark matter searches towards dwarf spheroidal galaxies
633 with Fermi-LAT, HAWC, H.E.S.S., MAGIC, and VERITAS”. in: *Proceedings of Science*.
634 Vol. 395. Mar. 2022. doi: <https://doi.org/10.22323/1.395.0528>.
- 635 [18] Tracy R. Slatyer. “Les Houches Lectures on Indirect Detection of Dark Matter”. In: *SciPost*
636 *Phys. Lect. Notes* (2022), p. 53. doi: [10.21468/SciPostPhysLectNotes.53](https://doi.org/10.21468/SciPostPhysLectNotes.53). URL:
637 <https://scipost.org/10.21468/SciPostPhysLectNotes.53>.
- 638 [19] Christian W Bauer, Nicholas L. Rodd, and Bryan R. Webber. “Dark matter spectra from
639 the electroweak to the Planck scale”. In: *Journal of High Energy Physics* 2021.1029-8479
640 (June 2021). doi: [https://doi.org/10.1007/JHEP06\(2021\)121](https://doi.org/10.1007/JHEP06(2021)121).
- 641 [20] Riccardo Catena and Piero Ullio. “A novel determination of the local dark matter density”.
642 In: *Journal of Cosmology and Astroparticle Physics* 2010.08 (Aug. 2010), p. 004. doi:
643 [10.1088/1475-7516/2010/08/004](https://doi.org/10.1088/1475-7516/2010/08/004). URL: <https://dx.doi.org/10.1088/1475-7516/2010/08/004>.
- 645 [21] B. P. Abbott et al. “Observation of Gravitational Waves from a Binary Black Hole Merger”.
646 In: *Phys. Rev. Lett.* 116 (6 Feb. 2016), p. 061102. doi: [10.1103/PhysRevLett.116.061102](https://doi.org/10.1103/PhysRevLett.116.061102). URL: <https://link.aps.org/doi/10.1103/PhysRevLett.116.061102>.
- 648 [22] R. Abbasi et. al. “Observation of high-energy neutrinos from the Galactic plane”. In: *Science*
649 380.6652 (June 2023), pp. 1338–1343.
- 650 [23] NASA Goddard Space Flight Center. *Fermi’s 12-year view of the gamma-ray sky*. website.

- 651 2022. URL: <https://svs.gsfc.nasa.gov/14090>.
- 652 [24] Marco Cirelli et al. “PPPC 4 DM ID: a poor particle physicist cookbook for dark matter
653 indirect detection”. In: *Journal of Cosmology and Astroparticle Physics* 2011.03 (Mar.
654 2011), p. 051. doi: [10.1088/1475-7516/2011/03/051](https://dx.doi.org/10.1088/1475-7516/2011/03/051). URL: <https://dx.doi.org/10.1088/1475-7516/2011/03/051>.
- 656 [25] A. U. Abeysekara et al. “Observation of the Crab Nebula with the HAWC Gamma-Ray
657 Observatory”. In: *The Astrophysical Journal* 843.1 (June 2017), p. 39. doi: [10.3847/1538-4357/aa7555](https://doi.org/10.3847/1538-4357/aa7555). URL: <https://doi.org/10.3847/1538-4357/aa7555>.
- 659 [26] A. Albert et al. “Dark Matter Limits from Dwarf Spheroidal Galaxies with the HAWC
660 Gamma-Ray Observatory”. In: *The Astrophysical Journal* 853.2 (Feb. 2018), p. 154. ISSN:
661 1538-4357. doi: [10.3847/1538-4357/aaa6d8](https://dx.doi.org/10.3847/1538-4357/aaa6d8). URL: [http://dx.doi.org/10.3847/1538-4357/aaa6d8](https://dx.doi.org/10.3847/1538-4357/aaa6d8).
- 663 [27] Giacomo Vianello et al. *The Multi-Mission Maximum Likelihood framework (3ML)*. 2015.
664 arXiv: [1507.08343](https://arxiv.org/abs/1507.08343) [astro-ph.HE].
- 665 [28] Marco Cirelli et al. “PPPC 4 DM ID: a poor particle physicist cookbook for dark matter
666 indirect detection”. In: *Journal of Cosmology and Astroparticle Physics* 2011.03 (Mar.
667 2011). ISSN: 1475-7516. doi: [10.1088/1475-7516/2011/03/051](https://dx.doi.org/10.1088/1475-7516/2011/03/051). URL: [http://dx.doi.org/10.1088/1475-7516/2011/03/051](https://dx.doi.org/10.1088/1475-7516/2011/03/051).
- 669 [29] Alex Geringer-Sameth, Savvas M. Koushiappas, and Matthew Walker. “Dwarf galaxy
670 annihilation and decay emission profiles for dark matter experiments”. In: *Astrophys.
671 J.* 801.2 (2015), p. 74. doi: [10.1088/0004-637X/801/2/74](https://dx.doi.org/10.1088/0004-637X/801/2/74). arXiv: [1408.0002](https://arxiv.org/abs/1408.0002)
672 [astro-ph.CO].
- 673 [30] Alex Geringer-Sameth, Savvas M. Koushiappas, and Matthew Walker. “DWARF GALAXY
674 ANNIHILATION AND DECAY EMISSION PROFILES FOR DARK MATTER EXPERI-
675 MENTS”. in: *The Astrophysical Journal* 801.2 (Mar. 2015), p. 74. ISSN: 1538-4357. doi:
676 [10.1088/0004-637X/801/2/74](https://dx.doi.org/10.1088/0004-637X/801/2/74). URL: [http://dx.doi.org/10.1088/0004-637X/801/2/74](https://dx.doi.org/10.1088/0004-637X/801/2/74).
- 678 [31] V. Bonnivard et al. “Spherical Jeans analysis for dark matter indirect detection in dwarf
679 spheroidal galaxies - Impact of physical parameters and triaxiality”. In: *Mon. Not. Roy.
680 Astron. Soc.* 446 (2015), pp. 3002–3021. doi: [10.1093/mnras/stu2296](https://doi.org/10.1093/mnras/stu2296). arXiv:
681 [1407.7822](https://arxiv.org/abs/1407.7822) [astro-ph.HE].